ANALOG JOINT SOURCE CHANNEL CODING FOR OPTICAL COMMUNICATIONS AND IMAGE TRANSMISSION

by

Sergio Matiz Romero

A thesis submitted to the Department of Electronics Engineering of the Pontificia Universidad Javeriana in partial fulfillment of the requirements for the degree of Master of Science in Electronics Engineering

Fall 2014

TABLE OF CONTENTS

LIST OF TABLES

LIST OF FIGURES

Chapter 1

INTRODUCTION

Analog joint source-channel coding (JSCC) has recently emerged as a coding scheme that works purely in the analog domain. In contrast to traditional digital systems where zeros and ones are coded and transmitted, analog JSCC takes analog input symbols and generates analog channel symbols without any processing in the digital domain. The Shannon separation principle states that the optimal communication system can be achieved by cascading optimal source coding and optimal channel coding [1], however, this has limitations in practice. First, it does not consider the system complexity. From Shannon's paper [1], it is known that approaching optimality requires infinite block lengths, which results in long system delays and high computational complexity. Moreover, if the signal to be sent is analog, quasioptimal digital systems would require powerful vector quantization and source coding. Second, the separation principle does not say anything regarding robustness against a change in the channel conditions. Channel codes are designed to protect data at a certain channel signal to noise ratio (CSNR). If the CSNR increases, the channel codes will over-protect the data, which leads to low efficiency. On the other hand, if the CSNR decreases, the channel codes will no longer offer sufficient protection, and this can lead to a breakdown in system performance. Our goal is to design low-complexity analog JSCC schemes that present low distortion in lossy compression and graceful degradation when the channel conditions change.

In digital systems based on the separation principle, the source encoder first eliminates redundancy in the data, and then the channel encoder adds controlled redundancy in order to protect the data. In JSCC, both procedures are done together. It is known that sending a Gaussian source into an AWGN channel without doing any

coding is optimal [2]. However, in most cases it is necessary to perform either bandwidth compression or bandwidth expansion. Many pioneering techniques have been proposed to solve this issue. They range from well known frequency modulation (FM) and pulse position modulation (PPM) for bandwidth expansion, to channel optimized vector quantizers (COVQ) [3] for bandwidth compression.

Interestingly, recent developed techniques, known as Shannon Mappings can meet our goal in both bandwidth compression and bandwidth expansion [4], [5], [6]. This scheme uses space filling curves to fill an n-dimensional space with a one dimensional curve to create a mapping of $\mathbb{R}^N \to \mathbb{R}$ or $\mathbb{R} \to \mathbb{R}^N$. By selecting the direction of mapping, one can achieve $N : 1$ bandwidth compression or $1 : N$ bandwidth expansion. This scheme has shown surprisingly good performance when dealing with lossy compression in AWGN channels, with a resulting distortion that is very close to the theoretical limit. Furthermore, this scheme presents graceful degradation when the real CSNR is lower than the one used for the system design [4]. Most of the work on non-linear curves for bandwidth compression focuses on ML decoding for high CSNR. Under these conditions, it is possible to analyze the system performance, and use this analysis to optimize the curve parameters [5], [7], [8]. ML decoding results in a performance close to the theoretical limits for diverse sources and high CSNR. This is extremely interesting, since the system complexity is much lower than that of a separated scheme. Furthermore, since long block lengths are avoided the delay is small. Nevertheless, ML decoding does not perform well for low CSNR. Quasi-optimal MMSE decoding and optimization for all CSNR values was studied in [6]. By optimizing the system parameters and performing MMSE decoding, it is possible to obtain a performance that close to the theoretical limits in the whole CSNR region.

It has been shown in the literature that analog JSCC systems using Shannon Mappings can outperform digital systems while requiring less complexity. Specifically, the advantages of analog JSCC over digital systems for wireless communications have been studied in [9], where a thorough comparison between analog JSCC systems and

digital systems for wireless channels is presented. One of the most interesting observations in [9] is that if scalar quantization is utilized in the digital system, then for a wide range of CSNRs its theoretical limit (i.e., assuming perfect source and channel coding/decoding) is about 0.5 dB worse than practical results obtained with the analog mappings using MMSE decoding.

The objective in this paper is to investigate the application of these mappings in wireless optical communications. Unlike AWGN channels, rigorous fundamental limits of optical channels are still unknown, therefore coding techniques for optical communications are less well developed. Moreover there is still a growing demand of optical communications for both analog and digital systems [10], [11]. Hence it becomes important to study the optical channel and develop advanced coding schemes.

This work focuses on infrared (IR) IM/DD systems where information is modulated on the intensity of lightwave and direct detection measures the power of lightwave, which is similar to a square law detector in RF communications [12]. Infrared communications are ideal for short-range indoor applications and offer several advantages over radio links. IR radiation penetrates through glass but not through walls or opaque barriers, therefore IR transmission can be confined to a room. Moreover, high-speed IR emitters and receivers are available in the market at low cost. By contrast, radio frequency communications can penetrate through walls generating interference between different links and are more susceptible to multipath distortion [13].

First, an introduction to analog JSCC using Shannon Mappings and its application in AWGN channels is provided, since the proposed scheme for the IM/DD wireless optical channel is a modified version of the ones used in [7] and [6] for data transmission over AWGN channels. Then the optical channel model is described in Section 2.4 and the real optical communication system for analog JSCC is introduced in Section 4. In this section, the IM/DD optical channel is also characterized since attenuation and nonlinearities have to be taken into account in real communication systems. In Section 4.5, the channel capacity and the capacity achieving distributions

are calculated based on the experimental results obtained from the channel characterization. Then, a novel scheme to overcome the nonlinear behaviours of the real channel is described in Section 5 and both simulation and experimental results are compared showing the effectiveness of the proposed scheme. In addition, the complexity of the proposed system is provided and compared to that of digital systems. To conclude this work, in section 5.2, image transmission using analog JSCC and compressive sensing (CS) is considered. This is done using the previously mentioned Shannon Mappings to encode the continuous amplitude CS measurements proceeding from an analog source and then transmitting them through the channel [14], [15], [16]. Both simulation and experimental results for image transmissions are shown.

<div align="center">

Chapter 2

THEORETICAL FRAMEWORK

</div>

2.1 Analog Joint Source-Channel Coding Using Shannon Mappings

The idea of using geometric curves for bandwidth expansion was first introduced by Shannon in 1949 [17]. Similar ideas were also studied by Kotelnikov in [18]. However, this research area had not been of much interest until the works of Ramstad and Chung, [4], [5]. The name Shannon Mappings was given by Ramstad in [4] to honor the idea from Shannon 60 years ago. In the past 10 years, several authors have performed research in this area. Topics related to 2:1 mappings include channel mismatch [7], quantization [19], and optimum minimum mean square (MMSE) decoding [6]. Other bandwidth compression/expansion ratios have been studied in the literature, including 1:2 mappings [8], 3:1, 4:1 and 3:2 mappings [20], and mappings with ratios between 1:1 and 1:2 [21]. Akyol *et al.* [22] studied the optimal mapping schemes for different bandwidth compression/expansion ratios and concluded that the Archimedes spiral is very close to the optimal mapping scheme for 2:1 bandwidth compression when optimal decoders are used. Mappings for distributed systems were introduced in [23]. The use of Shannon mappings to improve performance of compressive sensing was reported in [14]. Although a significant number of papers have been published in recent years, research in this area is still in its early stage.

2.2 Channel Capacity and Optimal Performance Theoretically Attainable (OPTA)

The channel capacity of an AWGN channel with mean 0 and variance σ_N^2 is

$$C = \frac{1}{2}\log_2\left(1 + \frac{P}{\sigma_N^2}\right) \tag{2.1}$$

where P is the power of the channel input and P/σ_N^2 is referred to as *channel signal-to-noise ratio* (CSNR).

The signal distortion D will be measured using the mean square error criterion:

$$D = E\{\epsilon^2\} = E\{(x - \hat{x})^2\} \tag{2.2}$$

where ϵ is the error and $\hat{x}$ is the recovered estimate of x.

From rate distortion theory, when zero mean Gaussian sources with variance σ_X^2 are considered, the rate distortion function is given by:

$$R(D) = \max \left\{ \frac{1}{2} \log_2 \left(\frac{\sigma_X^2}{D} \right), 0 \right\} \tag{2.3}$$

It is also known from information theory that when M source symbols are to be transmitted in N channel uses the following relationship must be always satisfied:

$$MR(D) \leq NC \tag{2.4}$$

$$\frac{M}{2} \log_2 \left(\frac{\sigma_X^2}{D} \right) \leq \frac{N}{2} \log_2 \left(1 + \frac{P}{\sigma_N^2} \right)$$

$$\frac{\sigma_X^2}{D} = SDR \leq (1 + CSNR)^{N/M} \tag{2.5}$$

SDR is known as *signal-to-distortion ratio*. The optimal performance theoretically attainable, OPTA, is obtained when equation (2.5) is satisfied with equality.

2.3 The Archimedes' Spiral and System Model for AWGN Channels

In the literature, different types of curves have been proposed according to the source distribution. In general, the idea is to encode an N-tuple of i.i.d source symbols into K channel symbols and then transmit them through a channel with noise variance σ_N^2. It is known that for i.i.d zero mean Gaussian sources 2:1 mappings using the

Archimedes' spiral can achieve quasioptimal performance [7], [6]. This work will focus on this particular type of curves.

The Archimedes' Spiral can be described by the following parametric form:

$$
\begin{cases}
x_1 = \dfrac{\Delta}{\pi}\theta\sin\theta \\[4mm]
\qquad\qquad\qquad\qquad \text{for } \theta > 0, \\[4mm]
x_2 = \dfrac{\Delta}{\pi}\theta\cos\theta
\end{cases}
$$

$$(2.6)$$

$$
\begin{cases}
x_1 = -\dfrac{\Delta}{\pi}\theta\sin\theta \\[4mm]
\qquad\qquad\qquad\qquad \text{for } \theta < 0. \\[4mm]
x_2 = \dfrac{\Delta}{\pi}\theta\cos\theta
\end{cases}
$$

The two source symbols (x_1, x_2) are mapped onto the closest point on the Archimedes' Spiral, as shown in Fig. 2.1, thereby generating the corresponding channel symbol represented by the angle θ.
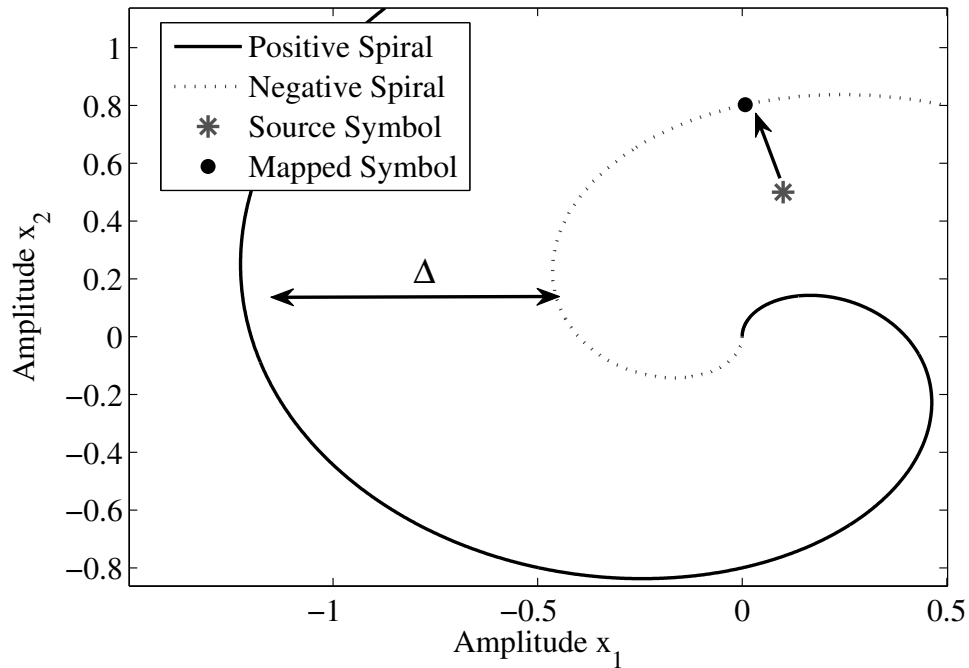

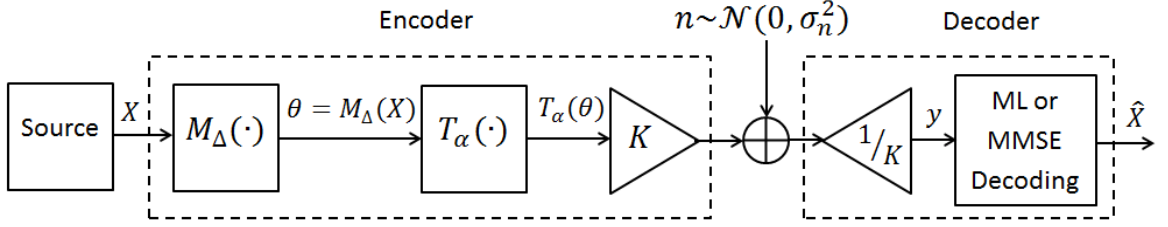Figure 2.1: Archimedes' Spiral mapping.

Figure 2.2: System model for AWGN channels.

The system model shown in Fig. 2.2 is utilized to transmit the analog symbols through the AWGN channel. After performing the mapping described above, represented by $M_\Delta(\cdot)$, a nonlinear function $T_\alpha(\cdot)$, often called *stretching function* [4], is used to reduce distortion. The transformation $T_2(\theta) = \mathrm{sign}(\theta)|\theta|^2$ was studied in [7] showing good performance close to OPTA. The general function $T_\alpha(\theta) = \mathrm{sign}(\theta)|\theta|^\alpha$ was studied in [6] and it was shown that the parameter α can be optimized together with Δ to obtain better performance, specially when the CSNR is low. Therefore in this article the latter approach will be used. Finally at the end of the encoder the normalization constant K is used to satisfied the constraint $E\{(Kz)^2\} \leq P$.

At the decoder the received signal is first multiplied by the constant $\frac{1}{K}$ and then ML or MMSE decoding is applied to obtain an estimated value $\hat{X}$. When ML decoding is used $\hat{X}$ is calculated as:

$$\hat{X_{ML}} = \arg\max_{X} p(y|X) \tag{2.7}$$

$$= \{X|X \in \boldsymbol{s} \text{ and } T_\alpha(\theta_X) = y\}, \tag{2.8}$$

where θ_X is the angle obtained after mapping X on the Archimedes' Spiral and s is the spiral-like curve. Therefore ML decoding can be performed by first applying the inverse function $T_\alpha(\cdot)^{-1}$ on the received symbol y and then the inverse mapping according to (2.6).

If MMSE decoding is chosen the $\hat{X}$ can be calculated in the following manner:

$$\hat{X_{MMSE}} = E\{X|y\} = \int Xp(X|y)dX \tag{2.9}$$

$$= \frac{1}{p(y)} \int Xp(y|X)p(X)dX. \tag{2.10}$$

The integral in (2.10) can only be calculated numerically since the function $p(y|X)$ involves the nonlinear transformation $M_\Delta(\cdot)$. However the value of the above integral can be accurately approximated by just performing additions and multiplications using the method described in [6].

2.4 The IM/DD Wireless Optical Channel Model

In IM/DD systems the information of the signal is modulated on lightwave intensity at the transmitter and is then recovered by direct detection of its power at the receiver. This paper focuses on optical wireless channels where an electrical signal is transformed into a lightbeam by a photodiode and then received by a photodetector (either a photodiode or phototransistor) which converts the received optical power back into an electric signal. The general block diagram of an optical wireless channel is represented in Fig. 2.3 following the scheme described in [24]. In this system the
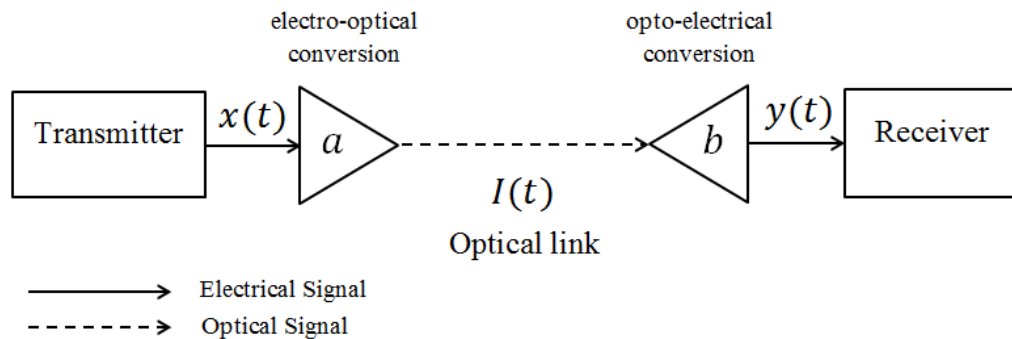
Figure 2.3: Optical wireless channel block diagram.

optical transmitter is driven by an electrical signal $x(t)$ (input signal) that produces the intensity $I(t)$. This can be written as $I(t) = ax(t)$ where a is the optical gain of the emitter given in $W/(A \cdot m^2)$. Since direct detection is performed by our system, the electrical signal produced by the photodetector $y(t)$ is proportional to the received intensity and can be written as $y = bI(t)$. If we take into account the channel response, the mathematical expression that describes the received signal $y(t)$ has the following form:

$$y(t) = |abx(t) * h(t) + n|, \tag{2.11}$$

where absolute values is due to the fact that intensity cannot be negative, the product ab is unitless and the function $h(t)$ represents the impulse response of the channel. The noise n is predominantly shot noise generated by the high intensity ambient light and by the Central Limit Theorem it can be modeled as signal-independent additive white Gaussian noise (AWGN) with variance σ_n^2 [25]. In our system model the signals are considered to be bandwidth-limited over the operation frequency range and the channel frequency response to be flat over that region. This leads to the following simplified channel model:

$$y(t) = |hx(t) + n|. \tag{2.12}$$

Where h represents the product ab. Since the physical quantity $x(t)$ is instantaneous optical power, this constrains all the transmitted amplitudes to be nonnegative.

$$(\forall t, x(t) \geq 0). \tag{2.13}$$

Chapter 3

SPECIFICATIONS

The proposed analog JSCC system meets the following specifications:

Performance close to OPTA

The performance of the system for the transmission of Gaussian random variables (simulations and experimental results) approaches the theoretical limits and the losses are less than 1dB for MMSE decoding.

Low Complexity

One of the main advantages of analog JSCC systems over digital systems is that their complexity is very low. The proposed scheme is more than 10 times less complex than the digital systems considered.

Feasibility

Several analog JSSC schemes using Shannon Mappings have been proposed in the literature. However, those systems have not yet been implemented and only simulations have been performed. In this work, the proposed analog JSCC system was implemented using a testbed. Furthermore, the experimental results approach the theoretical limits.

Image Transmission Capability

Image transmission of CS images using analog JSCC has been studied in [15] for AWGN channels. In this work these techniques are studied and new schemes are developed to allow the transmission of CS images over the IM/DD Wireless optical channel. Both simulations and experimental results are shown.

Chapter 4

DEVELOPMENTS

In this chapter the prototype designed to transmit data using analog JSCC is presented. First the opto-mechanical mount used to ensure the repeatability of the experiments is described and then the electronics are explained. Later, the real IM/DD wireless optical channel is studied and characterized since phenomena like fading and nonlinearities play an important role in real channels and have to be taken into account at the decoding stage. Moreover, the channel capacity of the IM/DD wireless optical channel is calculated using a generalization of the Blahut-Arimoto algorithm.

4.1   Opto-Mechanical Mount

High precision opto-mechanical components were used to ensure the repeatability of the experiments. A 60cm bench plate was set over four self-adjusting leveling feet to ensure stability. Two posts were located at each end of the bench plate to support both transmitter and receiver as shown in Fig. 4.1. In order to obtain high-precision alignment two adjustable detector mounts were attached to the posts to fix the optical components. Finally, the precision alignment was performed using a laser diode ensuring that the laser beam hit the optical device at the other end of the bench plate.

4.2   Electronics

Two optical infrared (IR) components that operate at a wavelength of 940nm were selected to establish the optical link. The transmitter used is a Vishay TSAL6100 high power IR GaAlAs/GaAs diode and the receiver a Vishay BPV11F silicon NPN phototransistor for enhanced gain at the receiver stage. The simplified schematic is
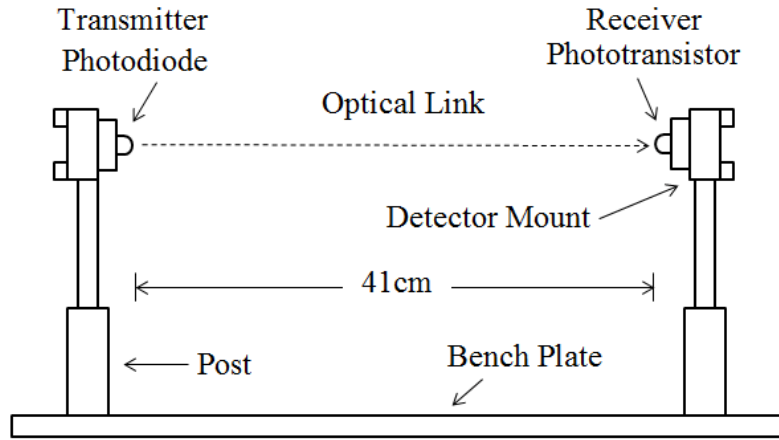
Figure 4.1: Opto-mechanical mount description.

shown in Fig. 4.2. The principle of operation is simple: A current source is controlled by the microcontroller DAC voltage output at the transmitter side, thereby controlling the optical power emitted by the photodiode. This relationship is represented as $i_x = kV_{ADC}$, where k is a constant given in A/V. At the receiver side the optical signal is converted into an electrical current i_p by the phototransitor. This current generates a voltage v_p then captured by the microcontroller ADC.
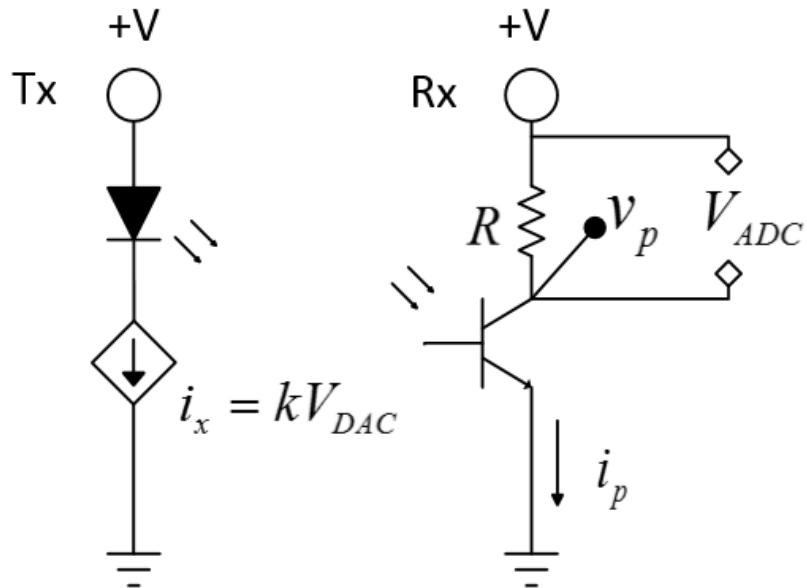
Figure 4.2: Simplified schematic.

4.3 System Operation

The system operation involves the circuitry shown in Fig. 4.2 a microcontroller and a PC. The data is first generated on the computer before transmission, this includes all the encoder stage or test signals used for the channel characterization. Subsequently the following steps are taken:

Step1: The data is transmitted from the computer to the microcontroller (MCU) by using the serial communications port (RS232 standard).

Step2: The data is converted into a voltage signal through the microcontroller DAC and then converted into electrical current by the voltage dependent current source i_x. This current produces the optical signal that is measured by phototransitor.

Step3: The optical signal is transformed into the current i_p by the phototransistor. This current generates the voltage v_p that is then measured by the microcontroller ADC.

Step4: the signal measured by the ADC is then sent out to the computer to be decoded and analysed.

4.4 Channel Analysis and Characterization

Real wireless channels and semiconductor devices present nonlinear behaviours that affect the performance of the overall system and represent a challenge at the decoding stage. Signal attenuation due to the distance between transmitter and receiver is also a factor to be taken into account since in some cases its effect can be severe and affect the signal reconstruction. For these reasons having some knowledge of the channel characteristics and behaviour becomes crucial in real communication systems.

4.4.1 Channel Attenuation and Nonlinearities

As mentioned before in section 2.4 the optical channel model can be represented by an equivalent electrical model, therefore, the characterization of the channel is performed measuring electrical signals. The channel attenuation coefficient h is obtained as $h = V_{ADC}/V_{DAC}$, thereby h is represented as the relationship between the voltage

output of the DAC that controls the photodiode and the voltage across the resistor R represented by V_{ADC} as shown in Fig. 4.2. For this experiment V_{DAC} is a known DC voltage signal set by the MCU at the transmitter and V_{ADC} is taken as the sample mean of a defined number of samples N taken by the ADC at the receiver.
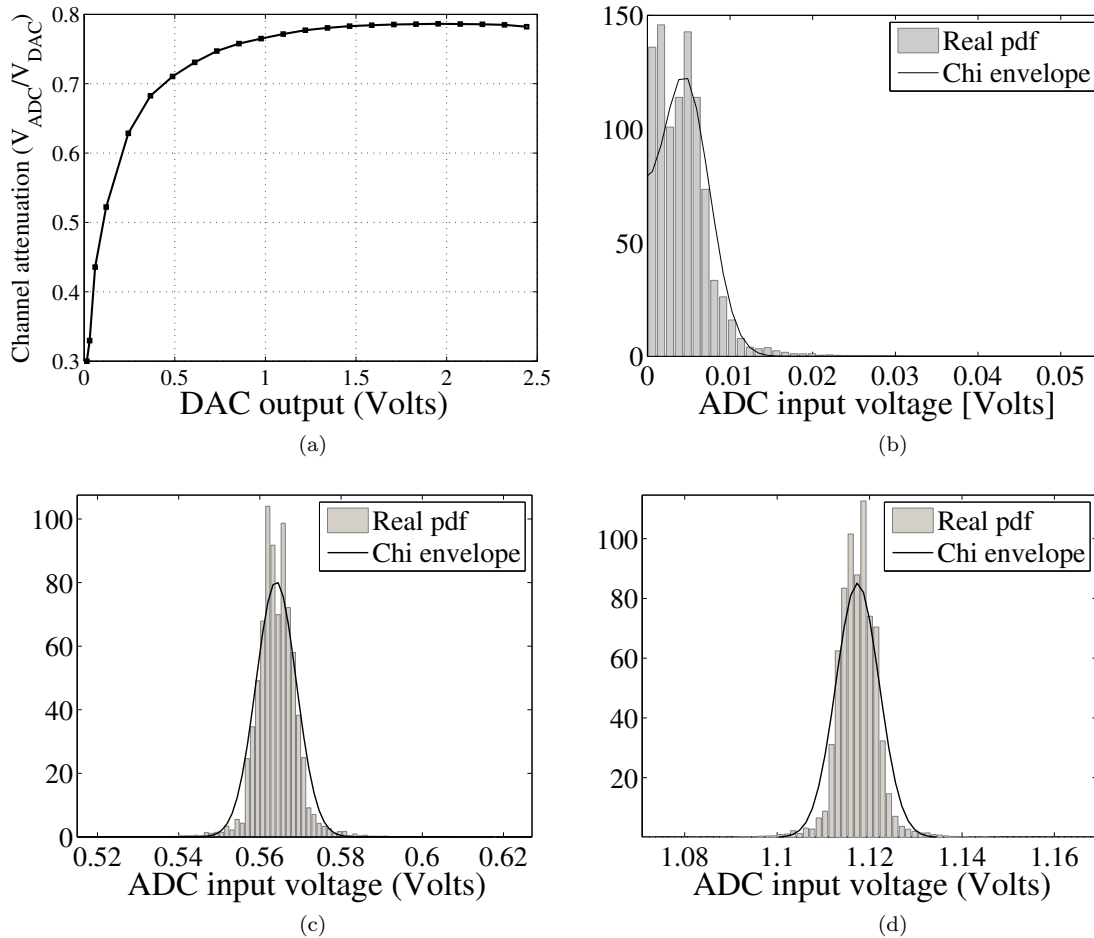
Figure 4.3: (a) Channel attenuation V_{ADC}/V_{DAC}, (b) Noise pdf for $V_{DAC} = 0.015V$, (c) Noise pdf for $V_{DAC} = 0.75$, (d) Noise pdf for $V_{DAC} = 1.50V$

The channel attenuation including the semiconductor nonlinear effects in both transmitter and receiver is shown in Fig. 4.3(a). When V_{DAC} is low the behaviour is highly nonlinear since the devices are not working entirely in their active region, however, as the V_{DAC} is increased the gain remains relatively stable for $V_{DAC} > 1V$.

4.4.2 Channel Noise

The maximum likelihood estimators were used to calculate the sample mean $\hat{\mu}$ and the variance $\hat{\sigma}^2$ of the received signal V_{ADC}. Despite the nonlinear behaviour of the channel the noise variance remains almost constant throughout the entire dynamic range of the device. Some of the experimental values obtained in the laboratory can be seen in Table 4.1.

$V_{DAC}[V]$	$\hat{\mu}[V]$	h	$\hat{\sigma}^2$
0.24	0.15	0.56	24.56×10^{-6}
0.73	0.54	0.72	24.74×10^{-6}
1.22	0.95	0.76	24.43×10^{-6}
1.71	1.34	0.77	24.83×10^{-6}

Table 4.1: Noise mean, variance and system gain for different values of V_{DAC}.

The pdf of the noise distributions for different values of V_{DAC} are shown in Fig. 4.3(b), (c) and (d). The pdf of the noise distributions for different values of V_{DAC} are shown in Fig. 4.3(b), (c) and (d). It can be seen that at the receiver the real noise resembles Gaussian noise, and for values close to 0 volts, as in Fig. 4.3(b), the distribution folds as a result of the optical channel constraints. This can be modeled using a Chi distribution of order 1 (the distribution of the absolute value of a Gaussian distribution). In Section IV, it will be shown that by approximating the system noise as zero mean Gaussian noise of the same variance and taking the absolute value of the received signal, the system can be modeled accurately and without any noticeable performance degradation.

4.5 Channel Capacity of the IM/DD Wireless Optical Channel

The channel capacity of the IM/DD wireless optical channel described by equation (2.12) cannot be calculated analytically. Therefore a generalization of the Blahut-Arimoto algorithm for continuous channels described in [26] is used.

Since the channel model is continuous the mutual information $I(X, Y)$ is given by:

$$I(X, Y) = \int_x \int_y p(x, y) \log \frac{p(x, y)}{p(x)p(y)} dxdy$$

$$= \int_x \int_y p(y|x)p(x) \log \frac{p(y|x)}{p(y)} dxdy \qquad (4.1)$$

where

$$p(y|x) = \frac{y^{1/2}}{\sigma_n^2 (hx)^{-1/2}} \, e^{-\frac{(y^2 + h^2 x^2)}{2\sigma_n^2}} I_{-1/2}\left(\frac{hxy}{\sigma_n^2}\right) \qquad (4.2)$$

which is the equation of a Chi distribution of order 1. This can be easily seen in equation (2.12) if the variable x is fixed and recalling that n is zero mean i.i.d white Gaussian noise.

Using the Blahut-Arimoto algorithm the equation $C = \max_{p(x)} I(X, Y)$ is solved. The gain coefficient h was also included in the calculation of the capacity to obtain the real channel capacity. The capacity achieving probability distributions $p(x)$ for the IM/DD wireless optical channel are shown in Fig. 4.4 and the capacity of the IM/DD wireless optical channel is depicted in Fig. 4.5.

Having characterized the real IM/DD optical channel the real system will be modeled accurately in Section 5. All the data transmissions of the experiments described in the following sections were done at a rate of 1KHz unless otherwise stated.
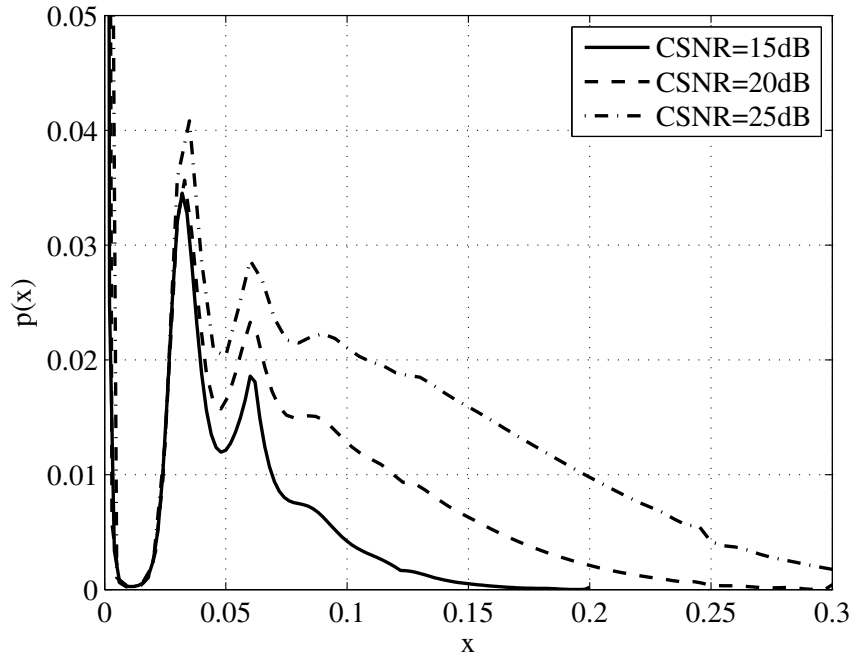
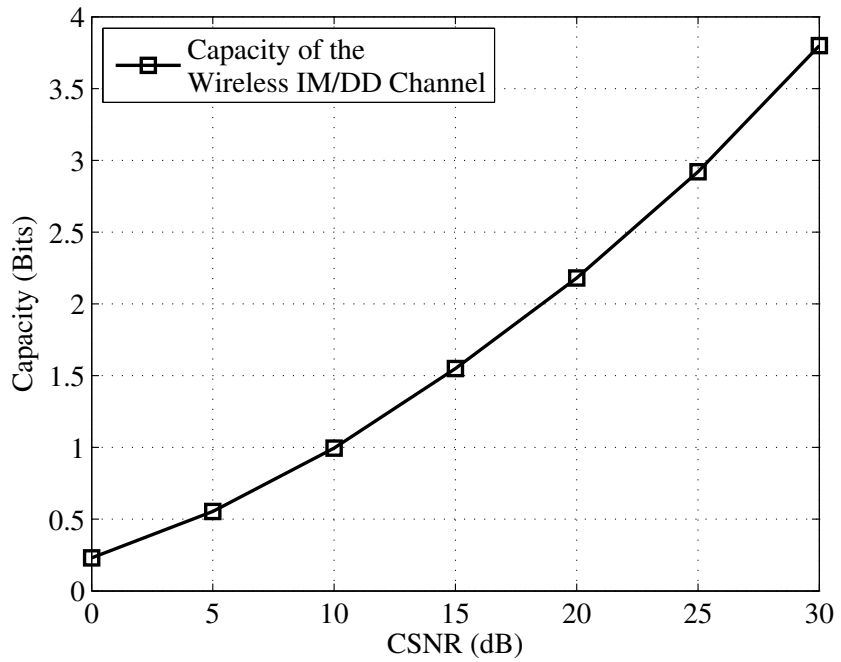Figure 4.4: Capacity achieving distribution $p(x)$.

Figure 4.5: Capacity of the IM/DD wireless optical channel.

<div align="center">

Chapter 5

ANALYSIS OF RESULTS

</div>

5.1 Analog JSCC over the IM/DD Wireless optical Channel

In this section the OPTA for the IM/DD wireless optical channel is derived. Then a new space filling curve is proposed based on the channel constraints and the new system model for the optical channel is presented. Both simulation and experimental results are shown and analyzed. Lastly, the complexity of the analog scheme is compared to that of digital systems.

5.1.1 OPTA for IM/DD Wireless Optical Channels

From the inequality $MR(D) \leq NC$ and (2.3) OPTA can be obtained as $\frac{\sigma_s^2}{D} \leq 2^{\frac{2NC}{M}}$. Since this work focuses on 2:1 mappings where $M = 2$ and $N = 1$ this can be further simplified to

$$\frac{\sigma_s^2}{D} \leq 2^C \tag{5.1}$$

5.1.2 Proposed 2:1 Mapping Scheme for the IM/DD Channel

In the IM/DD optical channel negative symbols cannot be transmitted due to the nature of the channel itself, therefore, the Archimedes' spiral described in Section 2.1 cannot be used directly. A single-arm spiral is used instead by only taking the positive arm of the original Archimedes' spiral. The rest of the elements in the system model shown in Fig. 2.2 remain the same. The single-arm spiral mapping can be represented as

$$\begin{cases} x_1(\theta) = \dfrac{\Delta}{\pi}\theta\sin\theta \\[4mm] x_2(\theta) = \dfrac{\Delta}{\pi}\theta\cos\theta \end{cases} \quad \text{for } \theta \geq 0 \tag{5.2}$$

<div align="center">

19

</div>

5.1.3   System Model for the Optical Channel and Simulation Results

The new scheme shown in Fig. 5.1 is proposed for the IM/DD optical channel. This new system model takes into account the intrinsic optical channel constraints.
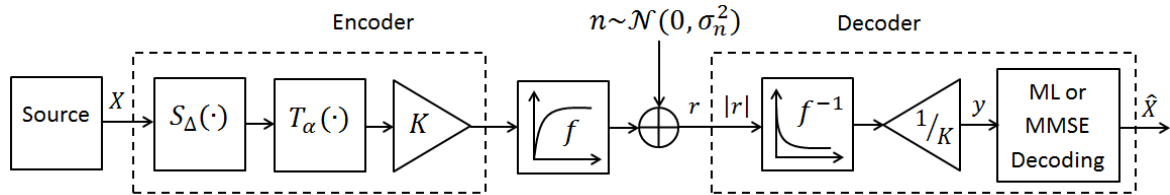

Figure 5.1: System model for the IM/DD wireless optical channel.

In this work we consider the transmission of zero-mean Gaussian sources with variance 1, ($\sigma_X^2 = 1$). The Archimedes' Spiral is replaced by the single-arm spiral mapping referred to as $S_\Delta(\cdot)$ in Fig. 5.1, thereby restricting the transmitted symbols θ to be nonnegative. The parameters α and Δ are optimized for each given CSNR as described in [6]. In order to mitigate the attenuation and the nonlinear behaviour of the real channel the new system model takes into account such factors by using a function f that simulates the channel attenuation as shown in Fig. 5.1. At the decoding stage, an inverse function f^{-1} is applied to the received symbols in order to alleviate the distorting effect.

The real channel is modeled as the combination of the attenuation function f applied to the transmitted symbols and the addition of zero mean Gaussian noise of variance σ_n^2 since the variance remains almost constant throughout the entire dynamic range of operation as shown in Table 4.1. Both ML and MMSE decoding were implemented by simulation to compare their performance. Following the same procedure as in [9], we calculated the theoretical limit for a digital system that utilizes scalar quantization, and include the corresponding curve in Fig. 5.2.

It can be seen that the curves for ML and MMSE decoding are close to each other for CSNR higher than 20dB, similar to the results obtained for the two-arm spiral mapping studied in [7] and [6]. However, for lower CSNR MMSE decoding performs better and the curves start to differ from each other significantly for CSNR lower than 15dB.
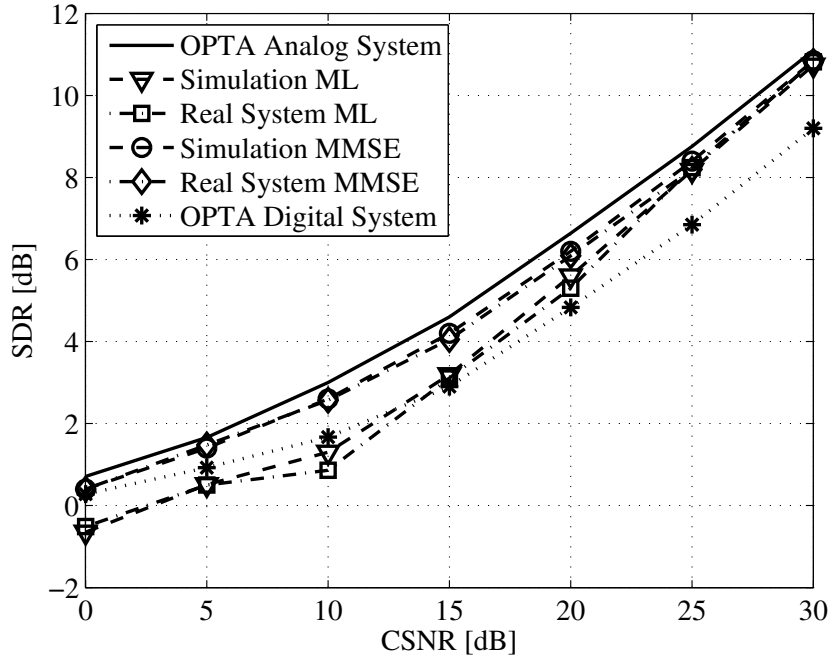
Figure 5.2: Performance of the simulated system vs the real system.

This leads us to think that in practical communication systems using this modulation scheme it is not necessary to use MMSE decoding unless the CSNR is low thereby reducing the complexity at the decoding stage. This fact will be used advantageously in Section 5.2 for image transmission since the real channel CSNR is greater than 20dB and ML decoding can be used instead of MMSE decoding obtaining good results and also reducing the processing time and complexity of the decoding stage significantly. Notice that the results of the real system performance follow almost exactly the simulation results. It can also be noticed that both the simulation and the real channel performance closely approximate the channel OPTA. It can also be observed in Fig. 5.2 that for the whole CSNR range, the theoretical limit (i.e., assuming perfect source and channel coding/decoding) of the digital system is worse than practical results obtained with the analog mappings using MMSE decoding. Even using ML decoding, the analog system outperforms the theoretical limit of the digital system for CSNR>15dB.

5.1.4 Complexity Results

In order to assess the complexity of the proposed scheme, a comparison between the number of computations required to encode/decode a source sample is presented for our system and for digital systems. The complexity of analog JSCC systems using spiral-like curves has been reported in [15], where the complexity of the analog system is calculated in terms of the number of computations required to encode/decode a source sample. Following the same procedure, the total complexity of the proposed system (including encoding and ML decoding) was calculated in this paper. Similarly, the complexity of decoding LDPC-like codes in terms of number of computations for digital systems has been reported in [27]. The results of both the proposed system and digital systems using LDPC-like codes can be seen in Table 5.1.

System	Multiplications	Additions	Comparisons
LDPC-like decoding	18700	5000	3800
Proposed system	359	279	187
Complexity of the proposed system as a percentage of LDPC-like decoding	1.92%	5.58%	4.92%

Table 5.1: Complexity per source sample for the decoding of a typical LDPC-like code and for the encoding/decoding of the proposed system using ML decoding.

Table 5.1 compares the complexity of the decoding of an LDPC-like code with the complexity of the encoder and decoder of the proposed system, both of them (LDPC-like decoding and proposed system) implemented on digital signal processors. The encoding complexity of the proposed system includes the calculation of the optimization function $M_\Delta(\cdot)$ for each sample, which is the greatest contributor to the overall complexity (the complexity of ML decoding is very small, as it is just a change of coordinates). Notice that the comparison in Table 5.1 penalizes the proposed system, since for the digital system only the decoding complexity of the LDPC-like code is included (the complexity of the source/channel encoder or the complexity of the source decoder is not included),

while for the proposed system it includes the end-to end encoding/decoding complexity (i.e., the whole number of operations necessary to transmit and decode data from transmitter to receiver utilizing digital signal processors). The reason we provide the comparison in this manner is to obtain a lower bound for the complexity of any digital system (based on either the separation principle or joint source-channel coding), as for any digital system the use of a very powerful channel code, such as an LDPC code, will be required.

5.2 Analog JSCC for Image Transmission over the IM/DD Wireless Optical Channel

It has been shown in previous works that it is possible to transmit images using analog JSCC applied to continuous amplitude compressive-sensing measurements coming from a CS encoder [4], [14], [15]. These techniques clearly outperform stand-alone CS systems where no encoding is used and the source symbols are sent directly through the channel [14]. Optimal energy allocation of the transmitted signal has also been studied in [15], aiming at PSNR improvements in the reconstructed images. In this section we adopt the scheme used in [15] for image transmission and extend it to the IM/DD wireless optical channel. Furthermore, a novel technique involving an additional nonlinear transformation is introduced, which leads to performance improvement.

5.2.1 Image Transmission over the IM/DD Wireless Optical Channel

The system model for image transmission is depicted in Fig. 5.3. First, the data is acquired through a CS encoder that produces kM continuous-amplitude symbols. The CS technique used in this paper is the one described in [28], which exploits the *a priori* information that natural images exhibit and takes into account their statistics and sparsity thereby acting as a source encoder [15]. Then, these symbols are encoded using the single-arm spiral mapping and the transformation $T_\alpha(\cdot)$ as shown in Fig. 5.1 producing M symbols. This step is represented by the Analog Channel Encoder block

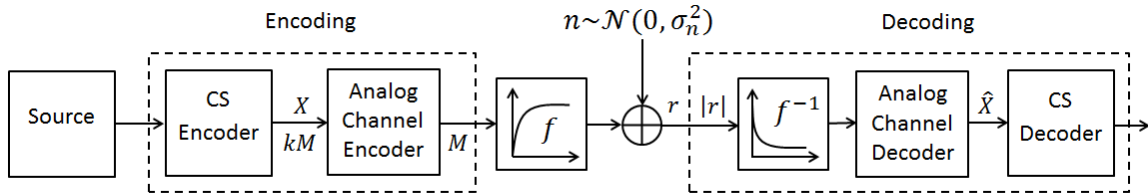in Fig. 5.3. The symbols are then sent through the IM/DD Wireless Optical Chan-

Figure 5.3: System model for image transmission.

nel and, at the decoding stage, the inverse transformation f^{-1} is applied to reduce distortion as mentioned in Section 5. Then ML decoding is applied to the incoming symbols and the output is decoded by a CS decoder to obtain the reconstructed image. Notice that for the 2:1 Shannon Mappings studied in this paper $k = 2$. The number of symbols to be transmitted is set to $M = 15000$ for the following experiments unless otherwise stated.

5.2.2 Nonlinear Transformation for Performance Improvement

It is known that the performance of systems using analog JSCC is highly dependent on the source probability density function (pdf) [4], [6]. Hence it becomes crucial to have control over the CS measurements coming from the CS encoder, which in general, are not Gaussian distributed. Previous works have tackled this problem by dividing the symbols to be transmitted in different energy bands [15], and in other cases these symbols are encoded and sent directly through the channel regardless of their pdf [14]. In this paper, based on the pdf of the CS measurements, a nonlinear transformation is proposed to reshape this pdf and improve the system performance.

5.2.2.1 CS Encoder Output Probability Distribution

The images to be encoded are 8-bit black and white images of 256×256 pixels. If no processing is done and the image is sent directly to the CS encoder the resulting output pdf is highly concentrated around zero and presents a higher value coefficient, usually two orders of magnitude higher than the others, related to the DC component

of the image. In order to mitigate this phenomenon, the image to be sent is normalized to values in the range $[-0.5, 0.5]$ before entering the CS encoder, thereby eliminating this high-valued coefficient, which in [15], is sent through the channel without encoding to improve performance in the image reconstruction.

5.2.2.2 The Nonlinear Transformation T_β

Having normalized the image as mentioned above, the nonlinear transformation $T_\beta(x) = \text{sign}(x)|x|^\beta$ is introduced into the system to modify the CS encoder output pdf as shown in Fig. 5.4.
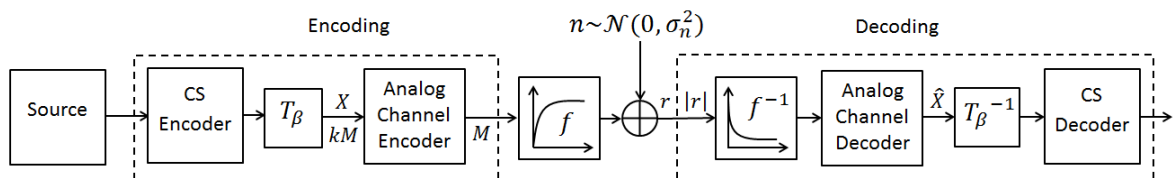

Figure 5.4: Proposed system model for performance improvement.

The original CS output pdf (when $\beta = 1$ and there is no modification) contains most of it measurements near the origin whereas the high-valued CS coefficients lay far away from it. This results in poor performance if the measurements are encoded without any modification. Therefore, the transformation $T_\beta(\cdot)$ for $\beta < 1$ increases the performance of the system significantly mitigating this effect and producing a better match between source and channel.

5.2.3 Simulation Results

In order to illustrate the potential of the proposed system a 256×256 "Boat" image was considered. The original CS encoder output pdf and the modified versions obtaining after using the transformation $T_\beta(\cdot)$ are depicted in Fig. 5.5.

Following the same procedure described in Section 2.1 the parameters α and Δ were optimized for each given β and for the different CSNR. The proposed scheme is compared with two schemes previously studied in the literature. A brief description of them is provided here for clarity.
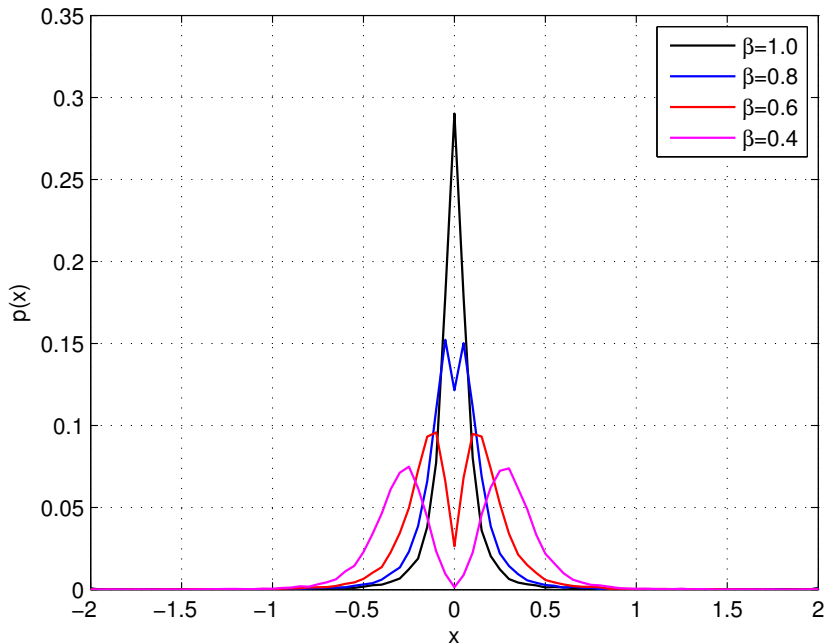
Figure 5.5: Probability distribution of the CS measurements after applying T_β using different values of β.

5.2.3.1 Energy Allocation Method

The energy allocation method, which is described in detail in [15], obtains the symbols proceeding from the CS encoder and then divides them in two energy bands. The first band consists only of the first symbol which is generally two orders of magnitude bigger than the others. The second band contains the rest of the symbols. Then the energy is distributed to the bands in order to increase the overall performance. The average power per symbol of the system remains the same before and after the energy allocation process.

5.2.3.2 No Energy Allocation Method

This method is studied in [14]. The symbols proceeding from the CS encoder are directly encoded using the spirals and then transmitted through the channel. There is no processing before encoding.
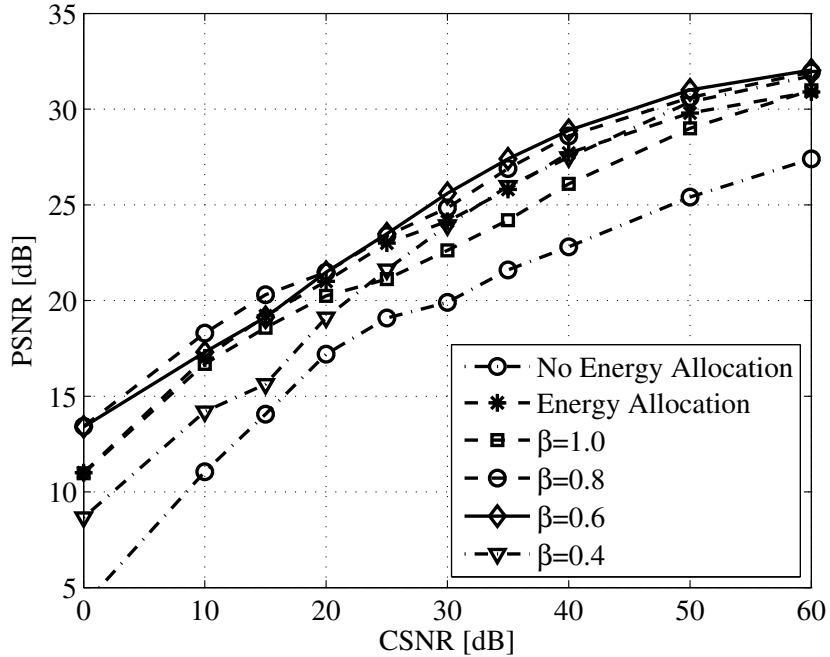
Figure 5.6: Performance results for the transmission of the image "Boat" using different methods

It can be seen in Fig. 5.6 that performance improvement after applying the transformation $T_\beta(\cdot)$ is significant. As β decreases the system performance experiences an increment over the whole CSNR range except when $\beta = 0.4$ and the pdf is severely modified. Intuitively, it can be said that β is a parameter that should be jointly optimized with α and Δ in order to obtain the optimal performance for every CSNR.

5.2.4 Experimental Results

One of the goals of this work is to study the applicability of analog JSCC in real communication systems, therefore it is of great interest to compare the simulation results with the experimental ones (which are obtained using the prototype described in Section 4). In order to do this the same 256×256 "Boat" image is considered and both simulation and experimental image reconstructions are presented in Fig. 5.7 for a CSNR=30dB. For this experiment, the encoding block shown in Fig. 5.4 was implemented using a standard processor. Then the encoded signal was sent to the
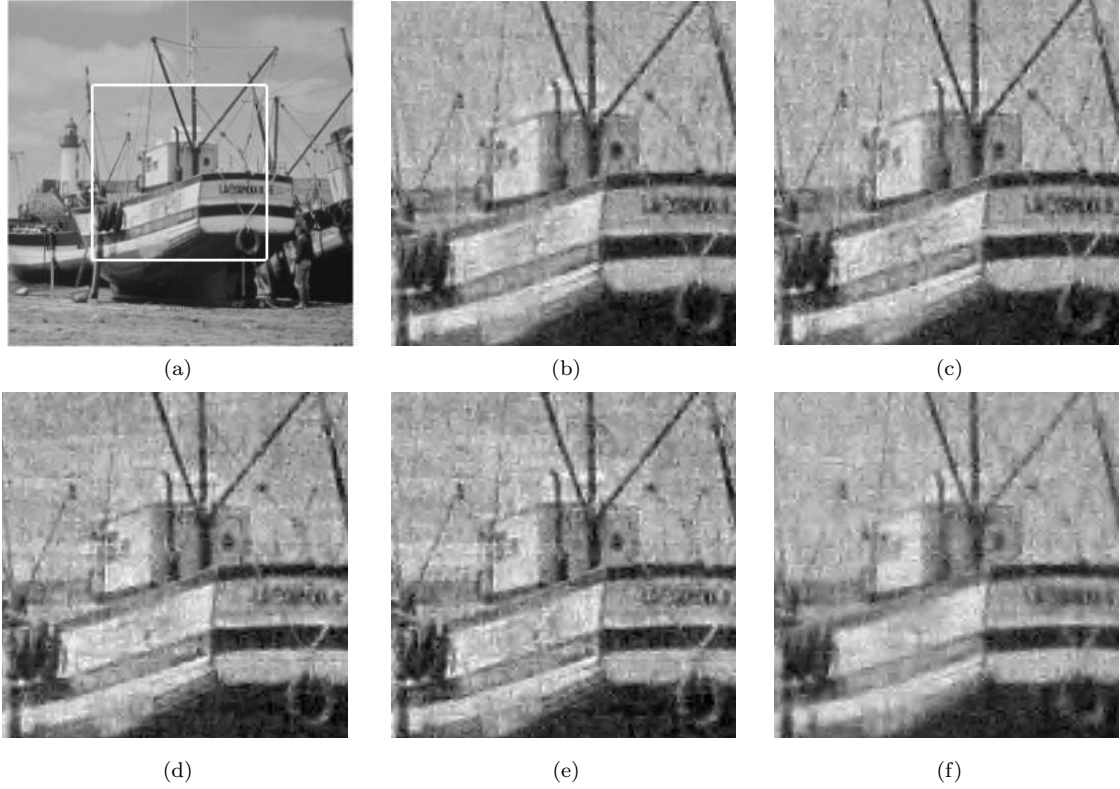
27

Figure 5.7: Original and reconstructed images for CSNR=30dB using the previously described methods.(a) Original *Boat* image (taken from The Waterloo Fractal Coding and Analysis Group image repository). (b) Simulation $\beta = 0.6$, PSNR=25.70dB. (c) Experimental $\beta = 0.6$, PSNR=25.20dB. (d) Simulation $\beta = 0.4$, PSNR=23.92dB. (e) Experimental $\beta = 0.4$, PSNR=23.63dB. (f) Simulation energy allocation PSNR=24.17dB.

microcontroller and transmitted through the optical channel.

It can be seen in Fig. 5.7(b) and Fig. 5.7(c) that the experimental and simulation results are very similar and the PSNR almost the same in both images. Likewise, Fig. 5.7(d) and Fig. 5.7(e) present similar distortion and the reconstructions show remarkable resemblance. Fig. 5.7(f) is the image reconstruction obtained using the energy allocation method [15]. Notice that, even though it presents a higher PSNR than the ones using T_β for $\beta = 0.4$, it does not preserve good edge quality and fine detail reconstruction. For this experiment, when the samples are sent directly through the channel after using the single-arm spiral mapping (if no energy allocation or T_β is used) the image cannot be adequately reconstructed. It also becomes evident in this

experiment that the transformation $T_\beta(\cdot)$ for $\beta = 0.6$ results in the best quality image reconstruction outperforming the other techniques in terms of PSNR and fine detail reconstruction.

Regarding implementation issues, the transformation $T_\beta(\cdot)$ is more convenient than the other methods being considered in this paper. The advantage lies in the fact that electronic components have peak power constraints and high CSNR conditions may become impossible to achieve if high-valued symbols cannot be transmitted due to hardware constraints. For instance, in the prototype considered in this paper it is necessary to rely on the transformation T_β in order to transmit images and obtain CSNR higher than 20dB. If no transformation is used, the values of some of the mapped symbols become so high that they cannot be transmitted by the real system.

Chapter 6

CONCLUSION

An analog JSCC communication system has been designed for the IM/DD wireless optical channel based on previous schemes used for AWGN channels. Based on experimental results, obtained using our prototype communication system, the IM/DD channel is characterized and its capacity calculated. Taking into account the nonlinear behaviour of the channel, a novel analog JSCC scheme is proposed to transmit data over the optical channel. The performance of the proposed scheme, in theory and practice, closely approaches the theoretical limits for ML and MMSE decoding when the parameters of the system are optimized. For the first time in the literature experimental results of analog JSCC communication systems over optical channels are obtained using a prototype. Furthermore, the proposed scheme is used for image transmission using the combination of compressive sensing and analog JSCC techniques. A new technique that involves a nonlinear transformation is introduced to the system model to improve its performance. The proposed system presents an excellent performance, while requiring very small complexity.

BIBLIOGRAPHY

[1] C. E. Shannon. A mathematical theory of communication. *Bell ystem Technical J*, 27(3):379–423, 1948.

[2] B.Rimoldi M. Gastpar and M. Vetterli. To code, or not to code: lossy source-channel communication revisited. *IEEE Trans. Inf. Theory*, 49(5):1147–1158, 2003.

[3] A. Fuldseth and T. Ramstad. Bandwidth compression for continuous amplitude channels based on vector approximation to a continuous subset of the source signal space. *IEEE Int. Conf. Acoustics, Speech,Signal Process. (ICASSP)*, 4:3093–3096, 1997.

[4] T. Ramstad. Shannon mappings for robust communication. *Telektronikk*, 98(1):114–128, 2002.

[5] S.Chung. On the construction of some capacity-approaching coding schemes. *Ph.D. dissertation, MIT*, 2000.

[6] J. Garcia-Frias Y. Hu and M.Lamarca. Analog joint source-channel coding using non-linear curves and mmse decoding. *IEEE Transactions on Communications*, 59(11):3016–3026, Nov. 2011.

[7] T.A Ramstad F. Hekland, G.E Oien. Using 2:1 shannon mapping for joint source-channel coding. *Proc. DCC*, Mar. 2005.

[8] P. Floor F. Hekland and T. Ramstad. Shannon-kotelnikov mappings in joint source-channel coding. *IEEE Trans. Commun*, 57(1):94–105, 2009.

[9] O. Freznedo, F.J. Vazquez-Araujo, M. Gonzales-Lopez, and J. Garcia-Frias. Comparison between analog joint source-channel coded and digital bicm systems. *IEEE International Conference on Communications*, 2011.

[10] A. Seeds and K. Williams. Microwave photonics. *J. Lightwave. Technol*, 24(12):46284641, 2007.

[11] A. Seeds and K. Williams. Scaling optical communications for the next decade and beyond. *Bell Labs Technical Journal*, 14(4):3–9, 2010.

[12] K. Kikuchi. History of coherent optical communication and challenges for the future. *Bell Labs Technical Journal.IEEE*, pages 107–108, 2008.

[13] J. M. Kahn and J. R. Barry. Wireless infrared communications. *Proceedings of IEEE*, 85(2):265–298, Feb. 1997.

[14] J. Garcia-Frias Y. Hu, Z. Wang and G. Arce. Non-linear coding for improved performance in compressive sensing. *43rd Annual Conference on Information Sciences and Systems. IEEE*, pages 18–22, 2009.

[15] J. Garcia-Frias I. Iglesias, B. Lu and G. Arce. Non-linear mappings for transmission of compressed sensing images. *48th Annual Allerton Conference on Communication, Control, and Computing (Allerton)*, pages 726–732, 2009.

[16] J. L. Paredes and G. R. Arce. Compressive sensing reconstruction by weighted median regression estimates. *IEEE Transactions on Signal Processing*, 59(6):2585–2601, Jun. 2011.

[17] C. E. Shannon. Communication in the presence of noise. *Proceedings ofthe IRE*, 37(1):10–21, 1949.

[18] V. Kotelnikov. The theory of optimum noise immunity. *New York: McGraw-Hill*, 1959.

[19] F. Hekland and T. Ramstad. Optimal rate-constrained transcoding for a 2:1 bandwidth reducing shannon mapping. *IEEE 7th Workshop on Signal Processing Advances in Wireless Communications*, pages 1–5, 2007.

[20] P. Floor and T. Ramstad. Dimension reducing mappings in joint source-channel coding. *Nowegian Signal Processing Sym. Workshop (NORSIG/IEEE)*, 2006.

[21] Y. Hu and J. Garcia-Frias. Optimizing power allocation in analog joint source-channel coding. *43rd Annual Conference on Information Sciences and Systems IEEE*, pages 72–76, 2009.

[22] K. Rose E. Akyol and T. Ramstad. Optimal mappings for joint source channel coding. *Information Theory Workshop (ITW). IEEE*, pages 1–5, 2010.

[23] T. Ramstad Emrah Akyol, Kenneth Rose. Optimized analog mappings for distributed source-channel coding. *Data Compression Conf., 2010 DCC. IEEE*, page 159168, 2010.

[24] S. Hranilovic and F.R Kschischang. Optical intensity-modulated direct detection channels: signal space and lattice codes. *IEEE Transactions on Information Theory*, 49(6):1385–1399, Jun. 2003.

[25] J.M Kahn and J.R Barry. Wireless infrared communications. *Proc. IEEE*, 85:263–298, Feb. 1997.

[26] O. Ndili and T. Ogunfunmi. Achieving maximum possible download speed on adsl systems. *IEEE Workshop on Signal Processing Systems*, page 407 411, Oct. 2007.

[27] Kjetil Fagervik and Arne Sjthun Larssen. Performance and complexity of low densityparity check codes and turbo codes. *NORSIG 2003*, Jun. 2013.

[28] Z. Wang and G. R. Arce. Variable density compressed sensing image sampling. *IEEE Transactions on Image Processing*, 9(1):264 270, Jan. 2010.